photonics

MDPI

Article

Tunable THz Graphene Filter Based on Cross-In-Square-Shaped Resonators Metasurface

Anton Zaitsev *, Alexander Grebenchukov * and Mikhail Khodzitsky

THz Biomedicine Laboratory, ITMO University, Saint-Petersburg 197101, Russia; khodzitskiy@yandex.ru

* Correspondence: a.zaytsev@niuitmo.ru (A.Z.); grebenchukov_a@mail.ru (A.G.)

Received: 20 September 2019; Accepted: 11 November 2019; Published: 12 November 2019

Abstract: The tunable terahertz (THz) Fano-resonant filter based on hybrid metal-graphene metamaterial was proposed. The optical parameters of metasurface with unit cell in the form of a cross-shaped graphene sheet in the center of a square gold ring were simulated by the finite element method using a surface conductivity model of a graphene monolayer. The narrowband modulation of the transmission by varying the Fermi level of the graphene and the position of graphene cross inside the metal ring was demonstrated. Simulation results were well explained theoretically using a three-coupled oscillator model. The proposed device can be used as a narrowband filter in wireless THz communication systems and sensing applications.

Keywords: graphene; terahertz filter; tunable metamaterial

1. Introduction

The radiation in THz (tunable terahertz) frequency range has recently turned into an active area of scientific research due to the creation of efficient THz sources and detectors [1]. There are almost no natural sources of such artificial radiation, therefore, the external noise in this range is low. THz radiation has a non-ionizing nature and is highly absorbed by conductors, but easily passes through most dielectrics. Due to these properties of THz radiation, there are actively developed systems for THz spectroscopy and diagnostics, visualization and imaging, as well as ultra-high-speed wireless communication systems [2,3]. Efficient and inexpensive components coupled with a high response speed that can control THz radiation are required for these systems. The usage of metamaterials instead of natural materials allows for the effective control of radiation in a wide frequency range due to its special properties. The resonant frequency of metamaterial is uniquely determined by the structural cell geometry. The cell of an active metamaterial usually consists of metal patterns and semiconductor layers, so the real-time manipulation of THz radiation can be achieved [4]. However, semiconductor-based metamaterials generally lack dynamically-active tunability [5]. Two-dimensional materials are regarded as a promising alternative for the basis of active metadevices [6]. Graphene is the best-known two-dimensional semiconductor material that has attracted a lot of interest since its discovering in 2004 [7]. Graphene is chemically stable, flexible, and almost defect-free with high carrier mobility and responsibility, as well as variable conductivity in the THz frequency range [8]. The conductivity of graphene can be changed by applying a bias voltage between metamaterial and graphene, as well as by infrared optical pumping or chemical doping [9]. The usage of such material in the structure of metamaterial allows one to achieve efficient and ultra-high-speed control of THz radiation. Currently, different hybrid structures based on graphene/metal have been proposed in recent works [10,11]. These devices have a low quality factor as they generally operate in a wide frequency band. That fact limits the implementation of such devices in several applications like precise sensing. The narrow linewidth and high Q-factor in the transmission spectrum of the metamaterial can be achieved by incorporating Fano resonances, originating from the coherent coupling (interference)

between discrete and continuous states [12,13]. These resonances show a sharp and asymmetric spectral line shape and produce a large strength and localization of the electromagnetic field. Integrating tunable 2D material into static metamaterial with Fano resonance allows one to achieve the active modulation of Fano spectral curves. In general, these devices can filter the spectrum of transmission or reflection of THz radiation, cutting out or skipping any frequency components determined by the geometry of the metamaterial unit cell. Operating at the frequency of the Fano resonance allows one to obtain an efficient narrowband tunable modulation.

In this work, we propose a tunable Fano-resonant THz filter based on the hybrid system consisting of cross-shaped graphene films in the center of square gold rings. According to the performed simulation, the amplitude of Fano resonance can be controlled through the shifting of graphene Fermi energy level with electrically biased ion-gel top-gate dielectric. Based on the three coupled oscillators model, the influence of graphene Fermi level changing on Fano spectral curves is theoretically studied. The obtained analytical curves are in good agreement with the simulation results. Furthermore, the influence of the metamaterial structure's geometrical parameters on its transmission spectra is investigated by numerical and theoretical analysis. The findings reveal the interaction between the graphene cross-shaped resonators and the surrounding metal ring, which opens a perspective towards the implementation of the proposed THz device for narrowband filtering and sensing applications.

2. Structure Description and Numerical Investigation

A schematic view of a graphene-based Fano-resonant filter unit cell is depicted in Figure 1. The proposed structure consists of a graphene cross inside a metallic (gold) square ring. In this structure, the width D and the length L of the graphene crosses are 45 µm and 100 µm, respectively. The structural parameters of metal square rings are defined as follows: R = 400 µm and K = 40 µm with the thickness of 0.5 µm, while the periodicity G of the combined structure is 770 µm. The 20 µm quartz film with a permittivity of $\epsilon = 3.75$ is chosen as a substrate. The thickness of the substrate is set so as to avoid the waveguide process. The thickness of the gold ring is determined by the skin depth at the used frequency and the technological possibility of the layer fabrication. Both these parameters are selected in accordance with the working frequency of the Fano-resonant filter.

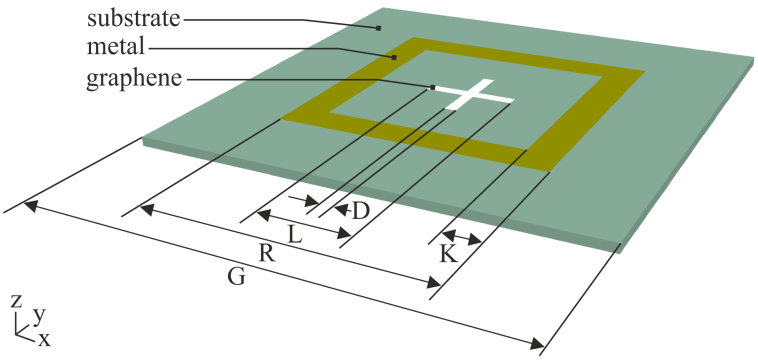

Figure 1. Scheme of the unit cell geometry: The graphene cross-like layer is located on the quartz substrate (with $\epsilon = 3.75$) in its center and is surrounded by a square gold ring. G is the size of the unit cell, R and K is the external size and width of gold ring respectively, and L and D is the length and the width of graphene cross-like layer respectively.

2.1. Conductivity Model of Graphene

The graphene is simulated as an isotropic infinitely thin layer through surface conductivity considering the contributions of interband and intraband transitions (Equations (1)–(3)) [14]:

$$\dot{\sigma} = \dot{\sigma}_{intra} + \dot{\sigma}_{inter}, \quad (1)$$

$$\dot{\sigma}_{intra}(\omega) = \left(\frac{e^2}{4\hbar}\right) \frac{8k_B T\tau}{\pi\hbar\left(1+\omega^2\tau^2\right)} \ln\left[1+\exp\left(\frac{E_F}{k_B T}\right)\right] + \\ +i\left(\frac{e^2}{4\hbar}\right) \frac{8k_B T\omega}{\pi\hbar\left(1+\omega^2\tau^{-2}\right)} \ln\left[1+\exp\left(\frac{E_F}{k_B T}\right)\right], \quad (2)$$

$$\dot{\sigma}_{inter}(\omega) = \left(\frac{e^2}{4\hbar}\right) \tanh\left(\frac{\hbar\omega - 2E_F}{4k_B T}\right) + i\left(\frac{e^2}{4\hbar}\right) \frac{1}{2\pi} \ln\left[\frac{(\hbar\omega + 2E_F)^2}{(\hbar\omega)^2 + (k_B T)^2}\right], \quad (3)$$

where i is the imaginary unit, k_B is the Boltzmann's constant, e is the charge of an electron, and $\hbar$ is the reduced Planck's constant. As seen from Equations (2) and (3), the surface conductivity $\dot{\sigma}$ depends on the environmental temperature T (293 K), the relaxation time τ (1 ps), the angular frequency ω, and the Fermi energy level of graphene E_F.

The proposed graphene-based metasurface can be electrically controlled with the ion-gel gate electrodes. The dependence of the Fermi energy on the gate voltage ΔV can be defined using the Equation (4):

$$E_F = \hbar v_F \left(\frac{\pi C \Delta V}{e}\right)^{1/2}, \quad (4)$$

where v_F is the Fermi velocity of charge carriers in graphene ($\sim 10^6$ m/s). For a 100 nm thick ion-gel layer the capacitance is $C = 2.45$ μF/cm^2 [15].

2.2. Numerical Simulation

The electromagnetic plane wave is polarized along the Y-axis and normally incidents along Z-axis. The boundary conditions are periodic along X-axis and Y-axis. The Drude formula was used to model the gold ring pattern. The graphene monolayer surface impedance dispersion was calculated using Equations (1)–(3) for the different values of the graphene Fermi energy levels in the range from 0.0 to 0.5 eV. Graphene was defined as the infinitely thin film. The electromagnetic simulations were performed using finite element method (FEM). Obtained S-parameters were used to extract the transmission spectra through relation $T(\omega) = |S_{12}|^2$.

In Figure 2, the transmission spectra of three different metasurface types are depicted: The graphene cross only (Figure 2a) with a graphene Fermi level of 0.5 eV, the metal ring (Figure 2b), and the combined structure consisting of the graphene cross inside the metal square ring (Figure 2c). It is seen that the 2nd resonance at 0.284 THz in the transmission spectrum of the metal-only metasurface is overlapped by the resonance originated from the cross-shaped graphene only metasurface. As a result, in the combined structure the amplification of graphene originated resonance is observed due to interference between the separate resonances arising from the graphene cross and the metal square ring.

In order to understand the nature of the arising resonances, we simulated the electric field distribution of the graphene cross-shaped metasurface, the metal square ring metasurface, and the integrated one at two frequencies associated with resonant dips in the transmission spectrum. As seen from Figure 2, the electric field distribution originated from the metal-only metasurface at the first resonance is similar to the electric field at the first resonance arising from the combined structure, while the field distribution at the second resonance from the hybrid structure is the result of the interference between resonant modes originated from the graphene-only and metal-only metasurfaces. The first peak refers to the resonance on the size of the metal ring, while the second one refers to the resonance on the whole structure and is determined by the coupling of the metamaterial cells within which the metal ring is located. The conductivity of graphene affects the parameters of both these resonances.

Then, the influence of the altering graphene Fermi level by electric gating on the transmission of the hybrid metasurface was investigated. The corresponding spectra are shown in Figure 3. As the Fermi energy of graphene increased from 0.0 eV to 0.5 eV, the transmission value at 0.275 THz decreased from 87% to 31% without any significant frequency shift, while the first resonance tended to red shift and undergo weak amplitude modulation from 15% to 2%. Furthermore, there was a high efficient tunability region between 0.225 THz and 0.250 THz where the amplitude modulation depth in the transmission spectrum could achieve 50%.

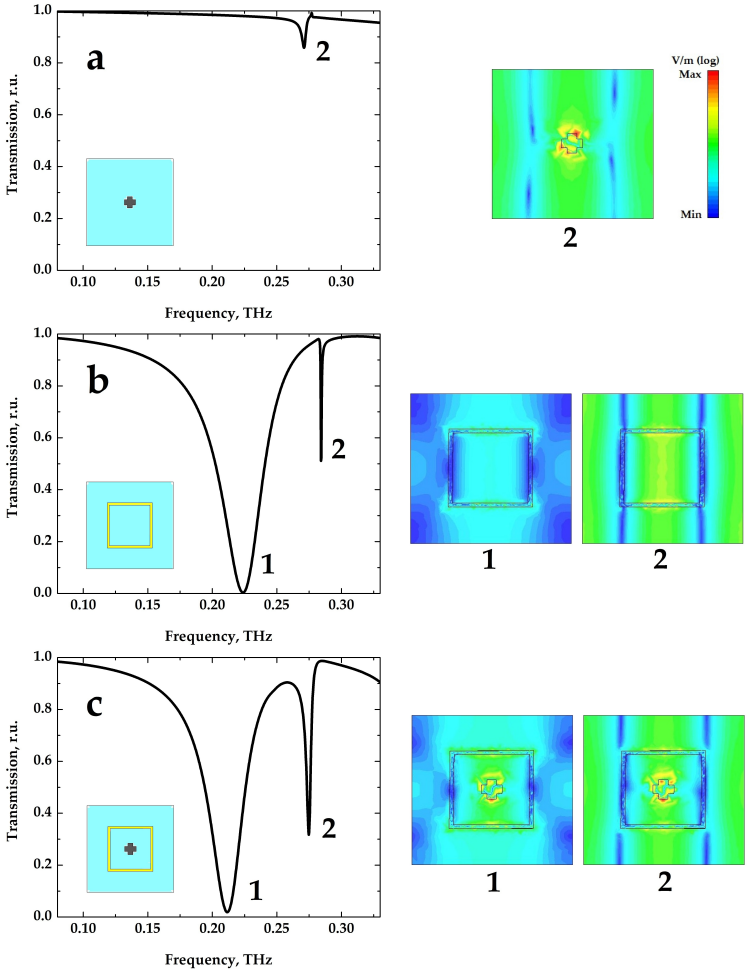

Figure 2. On the left side: Transmittance spectra of the filter in the absence of the gold ring with a fixed graphene Fermi level of 0.5 eV (**a**), in the absence of the graphene layer (**b**), and in case of the full Fano-resonant structure under electrostatic doping of 0.5 eV (**c**). On the right side: Corresponding electric field distributions.

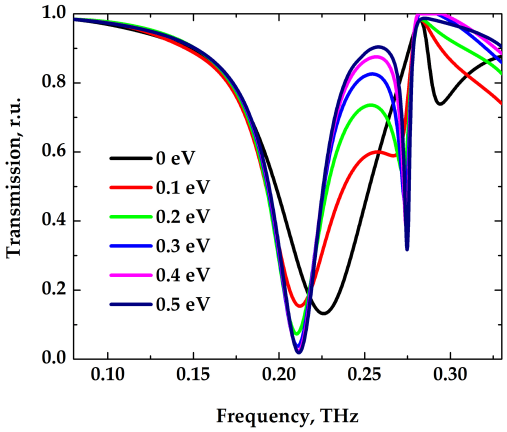

Figure 3. Transmission spectra of the filter for the different graphene Fermi level values from 0 eV to 0.5 eV (different gate voltage values).

3. Discussion

3.1. Coupled Oscillators Model Explanation

In order to understand the underlying physical mechanism of the observed effect, we adopted the classical coupled harmonic oscillator model under the incident electric field [16]. The transmission spectrum of the proposed structure can be described by three coupled second-order differential equations (see Equation (5)). The first two oscillators are related to resonances from the metal-only metasurface (Figure 2b) with two resonant frequencies ω_{m1} (0.2237 THz), ω_{m2} (0.2843 THz), and corresponding damping rates γ_{m1} (0.0384 THz), γ_{m2} (0.0008 THz). The third oscillator simulates the resonance from the graphene-only metasurface with a resonant frequency ω_g and damping rate γ_g (Figure 2a). The Q-factor is defined as $Q = \omega_g/\gamma_g$ and corresponds to a width of the resonant peak related to the central resonant frequency.

$$\begin{aligned} \ddot{x}_{m1} + \gamma_{m1}\dot{x}_{m1} + \omega_{m1}^2 x_{m1} + g_1 x_g &= f_{m1}e^{i\omega t}, \\ \ddot{x}_{m2} + \gamma_{m2}\dot{x}_{m2} + \omega_{m2}^2 x_{m2} + g_2 x_g &= f_{m2}e^{i\omega t}, \\ \ddot{x}_g + \gamma_g \dot{x}_g + \omega_g^2 x_g + g_1 x_1 + g_2 x_2 &= f_g e^{i\omega t}. \end{aligned} \tag{5}$$

Here, f_{m1}, f_{m2}, and f_g represent coupling with an external electric field, x_{m1}, x_{m2}, and x_g are resonant complex amplitudes that are expressed through the following expressions (Equation (6)):

$$\begin{aligned} x_{m1} &= C_{m1}e^{i\omega t}, \\ x_{m2} &= C_{m2}e^{i\omega t}, \\ x_g &= C_g e^{i\omega t}. \end{aligned} \tag{6}$$

Three oscillators have coupling strengths g_1 and g_2 which are represented in a complex form to model the phase retardation effect (Equation (7)) [17]. g_1 describes coupling between the low frequency broad resonance from the metal ring and resonance originated from the graphene cross. g_2 describes coupling between the high frequency narrow resonance from the metal ring and resonance originated from the graphene cross.

$$\begin{aligned} g_1 &= A_1 e^{i\varphi_1}, \\ g_2 &= A_2 e^{i\varphi_2}. \end{aligned} \tag{7}$$

After solving the equation system Equation (5) using Cramer's rule, the transmission spectrum can be derived as a sum of oscillator's square amplitudes $T = C_{m1}^2 + C_{m2}^2 + C_g^2$. Analytical fitting can be fulfilled using simulation data with different Fermi energy levels of graphene. All of the fitting parameters are presented in Table 1. It should be noted that negative values of A_2 denote that the coupling of oscillators is in the opposite phase.

Table 1. Fit parameters obtained from simulation.

E_f, eV	ω_g, THz	γ_g, THz	Q	A_1	A_2	φ_1	φ_2	f_{m1}	f_{m2}	f_g
0	0.2192	0.0385	5.7	0.9	−0.8	1.62π	0.08π	1	0.1	0
0.1	0.2632	0.0387	6.8	0.47	−0.7	1.85π	0.27π	1	0.1	0.03
0.2	0.2680	0.0112	24	0.47	−0.44	1.92π	0.3π	1	0.1	0.05
0.3	0.2692	0.0088	30.6	0.47	−0.34	1.93π	0.32π	1	0.1	0.08
0.4	0.2701	0.005	54	0.47	−0.3	1.94π	0.33π	1	0.1	0.1
0.5	0.2712	0.0037	85	0.47	−0.28	1.94π	0.34π	1	0.1	0.12

As shown in Figure 4, the theoretical calculations are in good agreement with the simulation data. The change of transmission value at the second high-frequency resonance with the graphene Fermi level increase can be attributed to rising of the real part of the second coupling coefficient A_2 and the increase of the coupling strength between the external electric field and the graphene cross f_g.

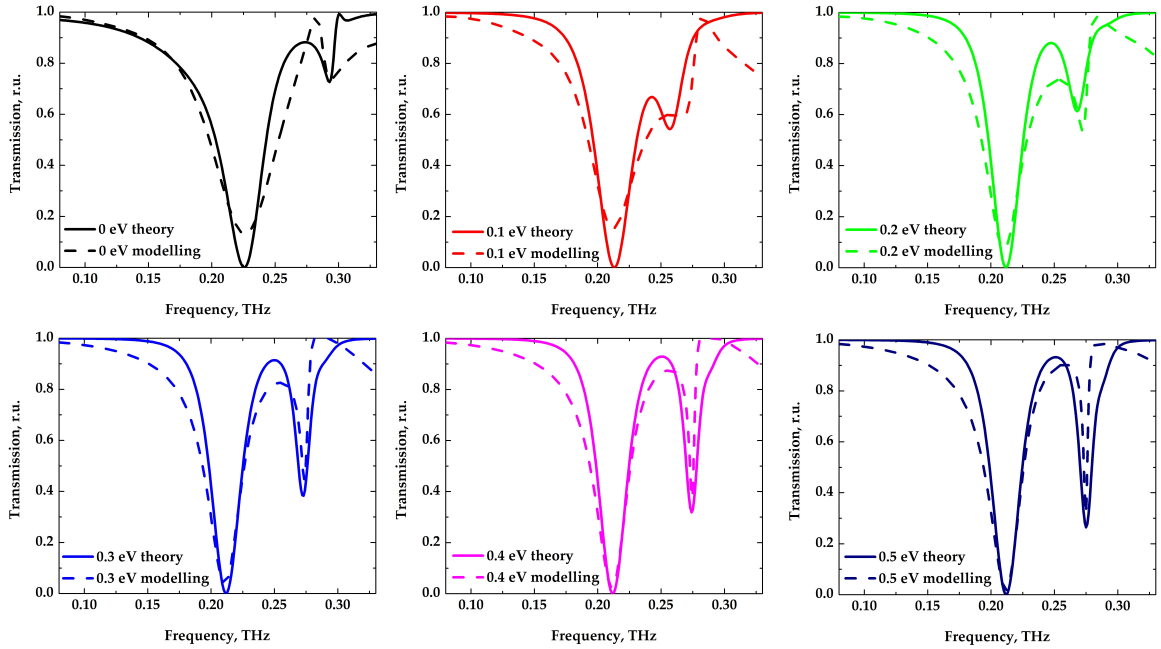

Figure 4. Transmission spectra for theoretical and numerical calculations with increasing graphene Fermi level values from 0 eV to 0.5 eV (different gate voltage values) for graphene-based filter.

3.2. *Influence of Graphene Cross Shift on the Transmission Spectra*

To investigate the influence of the graphene cross shift on the transmission spectrum of the proposed filter, we numerically simulated the transmission for different structure configurations with a fixed Fermi level of graphene. We considered two more structure configurations with a broken symmetry. For the first case, the graphene cross shifted along one direction (along X axis) up to 100 µm. For the second structure configuration, the graphene cross shifted along two directions (along both X and Y axis) up to 100 µm each.

According to the performed simulation, the value of transmission at the second narrow resonance (0.275 THz) increased significantly from 0.31 to 0.73 with the graphene cross shifting along one axis up

to 100 μm from symmetry position and 0.78 with the graphene cross shifting along two axis at once on 100 μm each (Figure 5). Then, we applied the analytical fitting to simulated curves. As a result of the performed fitting, we revealed a large change in the complex coupling strength. The variation of fitting parameters for different structure configurations is shown in Table 2.

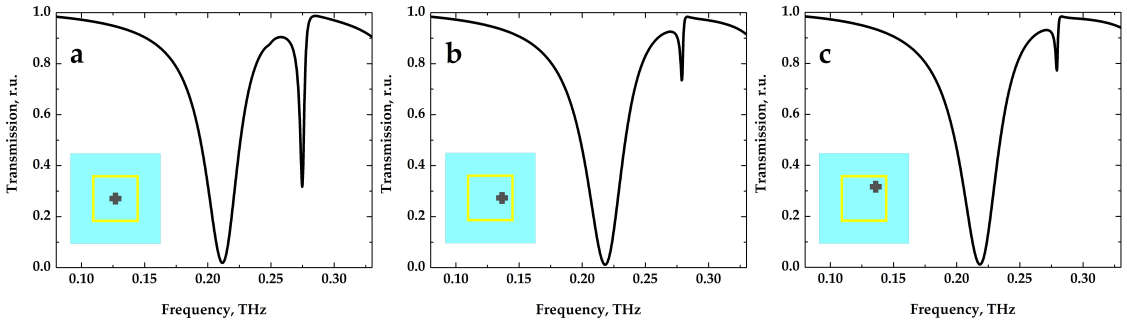

Figure 5. Transmission spectra of the filter with different unit cell structure: Original designed filter structure (**a**), structure with shifted graphene cross along one direction up to 100 μm (**b**), structure with shifted graphene cross along two directions up to 100 μm, and (**c**) graphene Fermi energy fixed at 0.5 eV.

Table 2. The fitting parameters for different graphene cross offset values.

Offset, μm	A_1	A_2	φ_1	φ_2
0–0	0.47	−0.28	1.94π	0.34π
0–100	0.3	−0.32	1.94π	0.51π
100–100	0.3	−0.35	1.94π	0.52π

It can be seen that the real part of the first coupling coefficient reduced after the cross shifting, while the real part of the second coupling coefficient increased in absolute value.

4. Conclusions

In conclusion, we proposed the tunable Fano-resonant filter based on a graphene monolayer. The numerical simulation results showed that by altering the graphene Fermi level, significant transmission modulation at certain frequencies could be achieved. To explain the underlying physics of the observed effect, we employed the three-coupled oscillators model. As a result, we revealed that with the increase of the graphene Fermi level from 0 ev to 0.5 eV the coupling coefficient A_2 between the resonators and coupling strength with the external electric field f_g tended to increase. In addition, symmetry breaking via the graphene cross shift led to an increase of the transmission value at the high-frequency resonance, which can be attributed to the change of the coupling strength between the metal ring and the graphene cross. The proposed filter and its analysis results may provide a guideline to develop graphene-based devices for wireless THz communication systems and sensing applications.

Author Contributions: Simulation, theoretical calculations, A.Z.; conceptualization, writing–original draft preparation, A.G.; supervision and editing, M.K.

Funding: This research was funded by the Government of Russian Federation grant number 08-08.

Conflicts of Interest: The authors declare no conflict of interest.

References

1. Nagatsuma, T.; Ducournau, G.; Renaud, C.C. Advances in terahertz communications accelerated by photonics. *Nat. Photonics* **2016**, *10*, 371. [CrossRef]
2. Yang, X.; Zhao, X.; Yang, K.; Liu, Y.; Liu, Y.; Fu, W.; Luo, Y. Biomedical applications of terahertz spectroscopy and imaging. *Trends Biotechnol.* **2016**, *34*, 810–824. [CrossRef] [PubMed]

3. Huq, K.M.S.; Jornet, J.M.; Gerstacker, W.H.; Al-Dulaimi, A.; Zhou, Z.; Aulin, J. THz communications for mobile heterogeneous networks. *IEEE Commun. Mag.* **2018**, *56*, 94–95. [CrossRef]
4. Xiao, S.; Wang, T.; Liu, T.; Yan, X.; Li, Z.; Xu, C. Active modulation of electromagnetically induced transparency analogue in terahertz hybrid metal-graphene metamaterials. *Carbon* **2018**, *126*, 271–278. [CrossRef]
5. Chen, H.T.; Padilla, W.J.; Zide, J.M.; Gossard, A.C.; Taylor, A.J.; Averitt, R.D. Active terahertz metamaterial devices. *Nature* **2006**, *444*, 597. [CrossRef] [PubMed]
6. Wang, M.; Yang, E.H. THz applications of 2D materials: Graphene and beyond. *Nano Struct. Nano Objects* **2018**, *15*, 107–113. [CrossRef]
7. Novoselov, K.S.; Geim, A.K.; Morozov, S.V.; Jiang, D.; Zhang, Y.; Dubonos, S.V.; Grigorieva, I.V.; Firsov, A.A. Electric field effect in atomically thin carbon films. *Science* **2004**, *306*, 666–669. [CrossRef] [PubMed]
8. Ferrari, A.C.; Bonaccorso, F.; Fal'Ko, V.; Novoselov, K.S.; Roche, S.; Bøggild, P.; Borini, S.; Koppens, F.H.; Palermo, V.; Pugno, N.; et al. Science and technology roadmap for graphene, related two-dimensional crystals, and hybrid systems. *Nanoscale* **2015**, *7*, 4598–4810. [CrossRef] [PubMed]
9. Hartmann, R.R.; Kono, J.; Portnoi, M.E. Terahertz science and technology of carbon nanomaterials. *Nanotechnology* **2014**, *25*, 322001. [CrossRef] [PubMed]
10. Jadidi, M.M.; Sushkov, A.B.; Myers-Ward, R.L.; Boyd, A.K.; Daniels, K.M.; Gaskill, D.K.; Fuhrer, M.S.; Drew, H.D.; Murphy, T.E. Tunable terahertz hybrid metal-graphene plasmons. *Nano Lett.* **2015**, *15*, 7099–7104. [CrossRef] [PubMed]
11. Jadidi, M.M.; Sushkov, A.B.; Gaskill, D.K.; Fuhrer, M.; Drew, H.D.; Murphy, T.E. Hybrid Metal-Graphene Terahertz Optoelectronic System with Tunable Plasmonic Resonance and Method of Fabrication. US Patent Application 15/735,662, 1 November 2018.
12. Lim, W.X.; Singh, R. Universal behaviour of high-Q Fano resonances in metamaterials: terahertz to near-infrared regime. *Nano Converg.* **2018**, *5*, 5. [CrossRef] [PubMed]
13. Grebenchukov, A.N.; Zaitsev, A.D.; Novoselov, M.M.; Kornilov, E.V.; Khodzitsky, M.K. Optically tunable Fano-resonant filter based on graphene. *Proc. SPIE* **2017**, *10343*, 103432V.
14. Weis, P.; Garcia-Pomar, J.L.; Rahm, M. Towards loss compensated and lasing terahertz metamaterials based on optically pumped graphene. *Opt. Express* **2014**, *22*, 8473–8489. [CrossRef] [PubMed]
15. Fang, Z.; Wang, Y.; Schlather, A.E.; Liu, Z.; Ajayan, P.M.; García de Abajo, F.J.; Nordlander, P.; Zhu, X.; Halas, N.J. Active tunable absorption enhancement with graphene nanodisk arrays. *Nano Lett.* **2013**, *14*, 299–304. [CrossRef] [PubMed]
16. Gallinet, B.; Martin, O.J. Ab initio theory of Fano resonances in plasmonic nanostructures and metamaterials. *Phys. Rev. B* **2011**, *83*, 235427. [CrossRef]
17. Taubert, R.; Hentschel, M.; Giessen, H. Plasmonic analog of electromagnetically induced absorption: Simulations, experiments, and coupled oscillator analysis. *JOSA B* **2013**, *30*, 3123–3134. [CrossRef]